Proceedings of the Institute of Acoustics

CALCULATION OF SOUND PROPAGATION FROM A POINT SOURCE OVER AN IMPEDANCE BOUNDARY

C. HOWORTH, K. ATTENBOROUGH, N. W. HEAP

THE OPEN UNIVERSITY, WALTON HALL, MILTON KEYNES, BUCKINGHAMSHIRE.

INTRODUCTION

Recently Chandler Wilde [1] investigated the problem of the reflection of a spherical wave from a homogeneous impedance plane. The representation of the field he derived is given by:

$$G_0(\underline{r},\underline{r}_0) = -\frac{e^{ikR_1}}{4\pi R_1} - \frac{e^{ikR_2}}{4\pi R_2} + P_\beta(\underline{r},\underline{r}_0) \tag{1}$$

for the geometry shown in

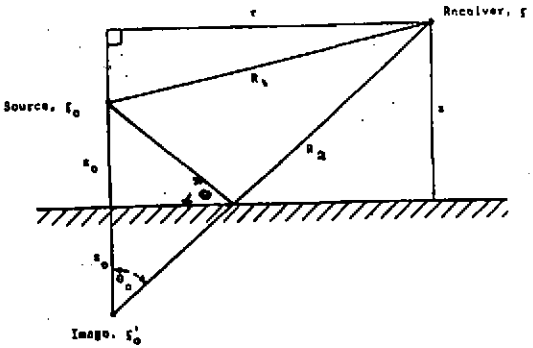

Figure 1: Geometry for reflection from an impedance boundary

$P_\beta(\underline{r},\underline{r}_0)$ accounts for the finite boundary admittance using a Hankel function representation. This term is presented in two integral forms which may are suitable for numerical calculation.

1)

$$P_\beta^{(\Gamma)} = \frac{k\beta e^{i\rho}}{2\pi}\int_0^\infty t^{-\frac{1}{2}}e^{-\rho t}f(t)ft \tag{2}$$

where β is the admittance, $\rho = kR_2$, and $k = \frac{2\pi f}{c}$ f is the frequency of interest and c the velocity of sound in air. This may be evaluated using Gauss-Laguerre quadrature provided that ρ is small, $|1-\beta| < \frac{1}{4}$ and $\leq \omega_e \leq \frac{3}{4}$. The integration is made difficult by $f(t)$ containing two Hankel functions with complex arguments.

2)

$$P_\beta = \begin{cases} \frac{ik\beta}{2\pi} e^{ip} \int_0^\infty \frac{e^{-st}}{\sqrt{-W(t)}} dt + \frac{k\beta}{2} H_0^{(1)}(kr\sqrt{1-\beta^2}) e^{-ik\beta(z+z_0)} & \text{if } \Im(\beta) < 0 \text{ and } \Re(a_+) < 0 \\ \frac{k\beta}{2\pi} e^{ip} \int_0^\infty \frac{e^{-st}}{\sqrt{W(t)}} dt & \text{otherwise} \end{cases} \quad (3)$$

with

$$W(t) \approx -(t - ia_+)(t - ia_-) = -t^2 + 2st(1 + \beta\gamma) + (\beta + \gamma)^2 \quad (4)$$

$$\text{and } a\pm \approx 1 + \beta\gamma \mp \sqrt{1-\beta^2}\sqrt{1-\gamma^2} \text{ and } \gamma = \cos\theta_0 \quad (5)$$

It is this second form that is used in the calculation which forms the basis of our comparisons. The integrand is evaluated using the D01AMF NAG routine which uses an adaptive procedure similar to the Gauss 7 point and Kronrod 15 point rules after transforming the integrand to the (0,1) form.

Chandler Wilde also reviewed several series approximations, when θ is large and concluded that the model proposed by Thomasson [2] is to be preferred to the model by Kawai et al [3] and Nobile [4].

In this paper we shall compare results from Numerical Integration with several of the more recent series approximations and with the widely used Weyl van der Pol model [5] for several typical impedance boundaries and geometries.

COMPUTER MODELLING OF PROPAGATION THEORY

The propagation models examined are

- *Weyl van der Pol* [5]
- Nobile and Hayek [4]
- Attenborough, Hayek and Lawther,[6]
- Kawai, Hidaka and Nakajima [3]
- Thomasson [2]
- Chandler Wilde (numerical integration) [1]
- Plane wave reflection coefficient model

WEYL VAN DER POL

The velocity potential representation is given by:

$$\phi_{tot} = \frac{e^{ik_1 R_1}}{4\pi R_1} + [R(\theta_0) + [1 - R(\theta_0)]F(w)] \frac{e^{ik_1 R_2}}{4\pi R_2}$$

with

$$F(w) = 1 + i\sqrt{\pi} w e^{-w^2} erfc(-iw)$$

$$w \simeq \frac{1}{2}(ikR_2)(\beta + \cos\theta)^2$$

$$R(\theta_0) = \frac{\cos\theta_0 - \beta}{\cos\theta_0 + \beta}$$

for small angles of incidence and low admittance surfaces . This form has become widely accepted when studying sound propagation. The complementary error function with a complex argument may be calculated using the approximations [7];

$$W(z) \simeq e^{-z^2} + \frac{2iz}{\sqrt{\pi}} \sum_{n=0}^{\infty} \frac{(-2z^2)^n}{1 \cdot 3 \cdot 5 \cdots (2n+1)} \text{ for all } z \tag{6}$$

$$W(z) = \frac{1}{\sqrt{\pi} z} \left(1 + \sum_{n=1}^{\infty} \frac{1 \cdot 3 \cdot 5 \cdots (2n-1)}{(2z)^2}\right) \tag{7}$$

as $z \to \infty$ and $\frac{\pi}{4} \leq arg(z) \leq \frac{\pi}{4}$

These have been used to develop a Pade approximant solution as suggested by Chandler Wilde .

NOBILE AND HAYEK

This series is produced so that the higher order terms are produced form the preceding terms using a recursion formulae.

The solution obtained by the authors is given by:

$$\phi(r,z) = \frac{e^{ikR_1}}{R_1} + \frac{e^{ikR_2}}{R_2} - \frac{4ik\beta e^{ikR_2}}{(\beta + \sin\psi)} \sum_{n=0}^{\infty} T_n [e_0 E_n + K_n] \tag{8}$$

$$T_n = \text{ Taylor coefficient } = \frac{1}{(2B)^n} \sum_{n=0}^{(n-2k)\geq 0} \binom{n-k}{k} a_{n-k} \left(\frac{4G}{H}\right)^{n-k} \tag{9}$$

$$\binom{n-k}{k} \text{ is the binomial coefficient} \tag{10}$$

$$e_0 = \frac{1}{2}\sqrt{\frac{\pi}{ikR_2}} e^{-\lambda^2} erfc(-i\lambda) \tag{11}$$

$$E_m = -BE_{m-1} + \left[\frac{(m-1)}{2ikr_2}\right] E_{m-2} \tag{12}$$

$$E_0 = 1,\ E_1 = -B \tag{13}$$

$$K_m = -BK_{m-1} + \left[\frac{(m-1)}{2ikR_2}\right] K_{m-2} \tag{14}$$

$$K_0 = 0.\ K_1 = \frac{1}{2ikR_2} \tag{15}$$

with

$$B = -i\sqrt{1 + \beta\sin\psi - \sqrt{1-\beta^2}\cos\psi} \text{ for } (Bi < 0,\ |re\surd > 0) \tag{16}$$

$$\lambda = \sqrt{ikR_2}\sqrt{1 + \beta\sin\psi - (1-\beta^2)^{\frac{1}{2}}\cos\psi} \tag{17}$$

$$G = -B^2 = 1 + \beta\sin\psi - \sqrt{1-\beta^2}\cos\psi \tag{18}$$

$$H = 1 + \beta\sin\psi + \sqrt{1-\beta^2}\cos\psi \tag{19}$$

$$a_m = \left[\frac{(\frac{1}{2} - m)}{m}\right] a_m - 1,\ a_0 = 1 \tag{20}$$

ATTENBOROUGH HAYEK AND LAWTHER

The authors use the contour integration method adopted by Paul [8] and steepest descents to calculate the field for both local and extended reacting surfaces at grazing incidence. The typographical errors were corrected Quartarraro [9]. The final field above a locally reacting surface is given by:

$$\phi_{tot} \simeq \frac{e^{ik_1R_1}}{4\pi R_1} + R(\theta_0)\frac{e^{ik_1R_2}}{4\pi R_2} - \frac{k_1\beta}{4}$$
$$\left[e^{(-\frac{x_0^2}{2})}erfc(-\frac{ix_0}{\sqrt{2}}) \times H_0^1\left[k_1r(1-\beta^2)^{\frac{1}{2}}\right]e^{ik_1r(1-\beta^2)^{\frac{1}{2}}}e^{ik_1R_2}\right] + V'(R) \tag{21}$$

with

$$\frac{(x_0)^2}{2} = ik_1R_2(1 + \beta\cos\theta_0 - (1-\beta^2)^{\frac{1}{2}}\sin\theta_0)$$

$$V'(R) \simeq \frac{\beta}{2\pi}\frac{e^{ik_1R_2}}{R_2(\beta+\cos\theta_0)}\left[\frac{1}{\sqrt{2}}\left(\frac{1+\beta\cos\theta_0}{(1-\beta^2)^{\frac{1}{2}}\sin\theta_0}+1\right)^{\frac{1}{2}}+\frac{1}{ik_1R_2(\beta+\cos\theta_0)^2}\right.$$
$$\left.\left[-(1-\beta\cos\theta_0)+\frac{\sin\theta_0(1-\beta^2)^{\frac{1}{2}}}{8\sqrt{2}}\times\left(1+\frac{1+\beta\cos\theta_0}{\sin\theta_0(1-\beta^2)^{\frac{1}{2}}}\right)^{\frac{3}{2}}\left(\frac{1+\beta\cos\theta_0}{\sin\theta_0(1-\beta^2)^{\frac{1}{2}}}+3\right)\right]\right] \quad (22)$$

KAWAI HIDAKA AND NAKAJIMA

The series is developed using a modified saddle point method. The authors claim an improved accuracy over the model due to Chein and Soroka [10], [11]. However it is suspected that the model will break down as the source-receiver separation decreases. The field above the impedance boundary is given by;

$$\phi = \frac{e^{ikR_1}}{R_1}+\frac{e^{ikR_2}}{R_2}+\left(R(\theta_0)-\frac{4\beta(1+\beta\cos\theta_0)}{(\beta+\cos\theta_0)^3}a\{F^*(kR_2a)-1\}\right)+\phi_s \quad (23)$$

with

$$\phi_s = \begin{cases} -2k\pi\beta H_0^1(kr\sqrt{1-\beta^2})e^{ik(z+z_s)\beta} & \Im(\beta)<0,\ \Re(a)<0 \\ 0 & \text{otherwise} \end{cases} \quad (24)$$

and

$$a = 1+\beta\cos\theta_0-\sqrt{1-\beta^2}\sin\theta_0 \quad (25)$$

for $\Re(\sqrt{1-\beta^2})>0$ and $kR_2 \gg 1$.

Although series expansions for $F^*(x)$ are given in the paper they are not used in the evaluation of the function.

THOMASSON

The series is produced using Watsons Lemma. The solution is satisfactory if the limit $kR_2 > 1$ exists. Whereas most other solutions apply both this and a further restriction. It is suggested by Chandler-Wilde that of the models discussed here the first three terms of the series will give the most accurate representation .

$$p = \frac{e^{ik_0R_1}}{-4\pi R_1}+\frac{e^{ik_1R_2}}{-4\pi R_2}+\frac{k_0\nu e^{ik_0R_2}}{2\pi}\int_0^\infty \frac{e^{-t}}{W^{-\frac{1}{2}}(t)}dt$$
$$+\frac{1}{4}(1-c)k_0\nu H_0^1(k_0r(1-\nu^2)^{\frac{1}{2}})\exp[-ik_0(z_s+z_R)\nu] \quad (26)$$

$$W(t) = (A^2+t)(B^2-t) \text{ and } A = [ik_0R_2(\gamma_0-1)]^{\frac{1}{2}} \text{ and } B = [ik_0R_2(1-\gamma_1)]^{\frac{1}{2}} \quad (27)$$

$$C = \begin{cases} +1; & -\frac{\pi}{2} \leq \arg(A) \leq \frac{\pi}{4} \\ -1; & \frac{\pi}{4} \leq \arg(A) \leq \frac{\pi}{2} \end{cases} \tag{28}$$

$$\begin{bmatrix} \gamma_0 \\ \gamma_1 \end{bmatrix} = -\cos(\theta_0)\nu \pm (1-\nu^2)^{\frac{1}{2}} \sin\theta_0 \tag{29}$$

$$\begin{bmatrix} R_2 \\ R_1 \end{bmatrix} = [r^2 + (z_r \pm z_s)^2]^{\frac{1}{2}} \tag{30}$$

$$r = [(x_s - x_r)^2 + (y_s - y_r)^2]^{\frac{1}{2}} \text{ and } \cos\theta_0 = \frac{(z_s + z_r)}{R_2} \tag{31}$$

the integrand is evaluated to give

$$P_R \sim \frac{Ck_0\nu e^{ik_0R_2}}{2\pi B} \sum_{m=0}^{\infty} \frac{(2m)!I_m}{(m!)^2(4B^2)^m} \tag{32}$$

for $\Re(\gamma_0) > 1$ with

$$I_0 = \sqrt{\pi}e^{A^2}erfc(A) \text{ and } I_1 = A + \left(\frac{1}{2} - A^2\right) I_0 \tag{33}$$

$$I_m = \left(m - \frac{1}{2} - A^2\right) I_{m-1} + (m-1)A^2 I_{m-2} \text{ for } m \geq 2 \tag{34}$$

PLANE WAVE REFLECTION COEFFICIENT MODEL (P.W.C.R.)

This wave model is often used as a simple model to predict sound propagation above ground of finite impedance.

$$\phi_{tot} = \frac{e^{ik_1R_1}}{4\pi R_1} + [R(\theta_0)]\frac{e^{ik_1R_2}}{4\pi R_2}$$

RESULTS

The level difference spectra, i.e. the transfer magnitude of function between two microphones the lower one being close to ground level, is examined for a range of geometries and impedances.

The difference in magnitude of the level difference spectra between the numerical integration model and the asymptotic series models is shown below together with the geometry used and the impedance of the surface. The impedances were found using the Rayleigh–Attenborough model [12], [13].

REFERENCES

CONCLUSIONS

As can be seen for the range of parameters shown the model proposed by Weyl and Van der Pol is quite suitable for the conditions encountered when characterizing the ground surface. Even for values of kR_2 of unity the Weyl van der Pol model gives a suitable prediction.

References

[1] Simon Neil Chandler-Wilde. PhD thesis, University of Bradford, 1988.

[2] S.I. Thomasson. *Acustica*, 45:122–152, 1980.

[3] T. Kawai, T. Hidaka, and T. Nakajima. *Journal of Sound and Vibration*, 83(1):125–138, 1982.

[4] M.A. Nobile and S.I. Hayek. *Journal of the Acoustical Society of America*, 78(4):1325–1336, October 1985.

[5] K. Attenborough. *Applied Acoustics*, 24:289–319, 1988.

[6] K. Attenborough, S.I. Hayek, and J.M. Lawther. *Journal of the Acoustical Society of America*, 68(5):1493–1501, November 1980.

[7] M. Abramowitz and A.G. Stegun, editors. Dover Publications Inc., 1970.

[8] D.I. Paul. *Journal of the Acoustical Society of America*, 29:1102–1109, 1957.

[9] L.R. Quartarraro. Master's thesis, Pennsylvania State University, 2000.

[10] C.F. Chein and W.W. Soroka. *Journal of Sound and Vibration*, 43:9–20, 1975.

[11] C.F. Chein and W.W. Soroka. *Journal of Sound and Vibration*, 69:340–343, 1980.

[12] Attenborough K. *Journal of Sound and Vibration*, 4:521–544, 1985.

[13] Attenborough K. *Journal of the Acoustical Society of America*, 73:785–799, 1983.

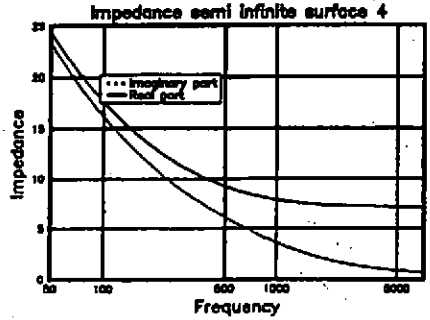

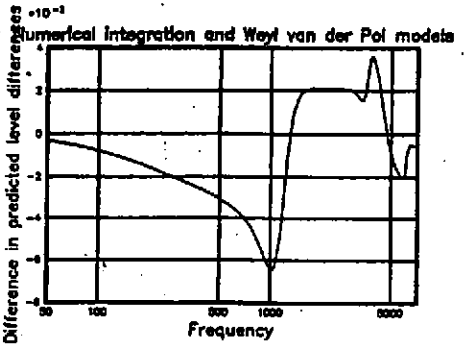

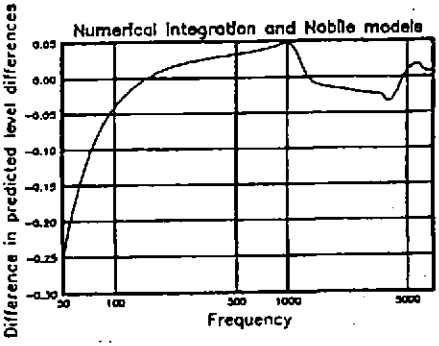

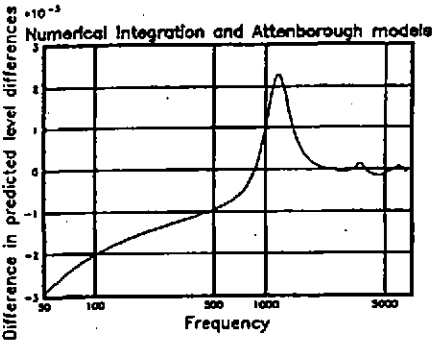

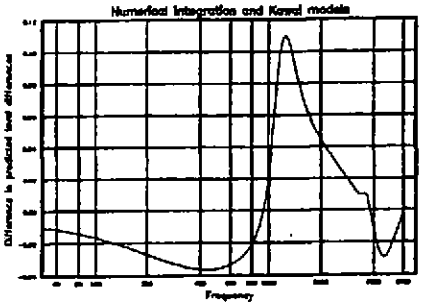

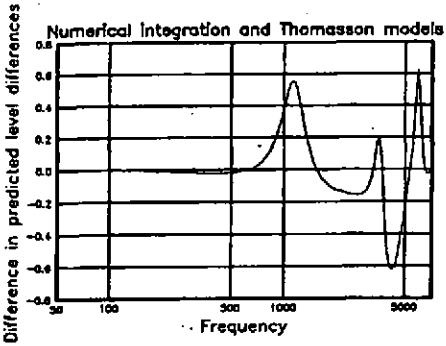

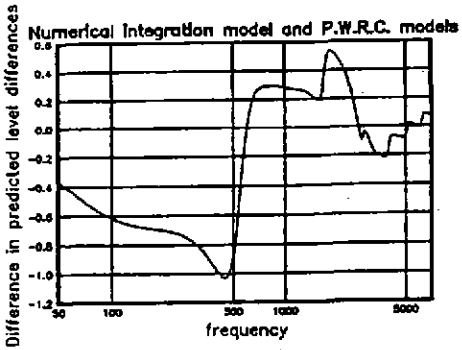

Geometry

Source Height=0.2m
Top Receiver Height=0.05m
Bottom Receiver Height=0.2m
Separation=0.5m

Figure 2: results for semi infinite surface 4

Proceedings of the Institute of Acoustics

THE GROUND WAVE IN OUTDOOR SOUND PROPAGATION

Johann Wempen

Fachbereich Physik, Universität Oldenburg, Postfach 2503, D–2900 Oldenburg, Fed.Rep.Germany

The prediction of sound propagation outdoors has often to deal with the case of nearly grazing incidence. The ground influence for this case is described with the theory of spherical wave propagation [1] by taking into account the impedance of the specific grounds. The theory predicts the occurance of a ground wave, propagating near the surface and depending sensitively on the properties of the ground. The original intention of the work presented here was to deduce effective impedances of several outdoor grounds for nearly grazing incident sound, including a comparision with those for larger grazing angles. During the work, the question of the influence of meteorological effects, i.e. wind– and temperature gradients, which are well known to establish in opposite ways during day and night [2], accured. Their influence on grazing sound propagation is a phenomenon not clarified until now. These gradients had been regarded as minor effects for sound propagation at smaller distances (up to 100 m), but it is shown, that the properties of the ground wave are sensitive to meteorological effects. Sound speed gradients above the ground have a strong influence on sound propagation, even over small distances of a few decameters.

THE INFLUENCE OF METEOROLOGY

The sound field above a flat and homogenous (as far as possible) lawn surface was measured twice on a sunny winter day. The first measurement was taken at noon with a strong negative temperature gradient expected, the second measurment was done shortly before sunset, where the temperature gradient had turned positive. The positive or negative temperature distribution was checked with a handheld thermometer.
Slow winds (wind speeds from zero to about 2 m/s) were partly present during the measurements. The noon measurement was taken upwind, the evening measurement downwind, in order to assure, that occuring wind speed gradients did rather increase than destroy the effects of the corresponding temperature distribution.
The sound field, emitted by a source elevated 40 cm above ground was picked up in three different heights (0.4 m, 0.8 m, 1.6 m), consequtively in four different distances (12.5 m, 25 m, 50 m, 100 m). The measuring technique is described in [3], it deliveres functions of the frequency dependent magnitude and phase of the excess attenuation relative free propagation of spherical waves.

Measurements of excess attenuation

Fig. 1 shows measured magnitudes and phases of the excess attenuation in 0.4 m height and four distances for the noon measurement. Low frequencies are transmitted from source to receiver without losses, $|H|$ is about +6dB (dashed lines), indicating a perfect reflection for any measured distance. This low frequency region is dominated by the ground wave, its low pass behaviour is sensitively depending on the properties of the ground. The cut–off frequency decreases slowly with increasing distance, the marked ground dip gets deeper. The reincrease of the magnitudes towards high frequencies is due to positive interference of direct and reflected waves, caused by the finite difference of the path lengths of direct and ground reflected waves. The measurement over 50 m shows a stronger decrease of the path length difference than expected from geometry (linear decrease), it even tends to zero for the 100 m position, where practically no sound of high frequency is transmitted to.
The phase functions shown below represent the phase lag of the total sound signal relative to spherically diverging waves. They are determined except an unknown linear part (time delay between

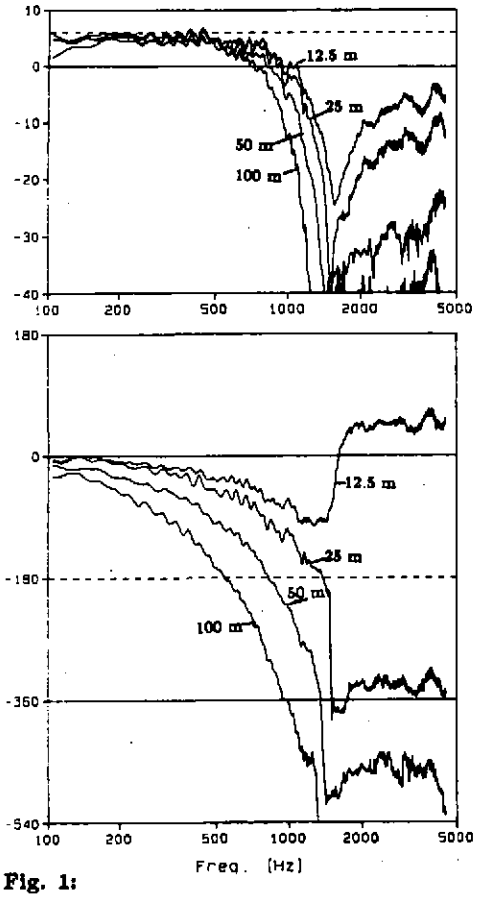

Fig. 1:
Magnitude of the excess attenuation function for grasing sound propagation along a lawn surface during day conditions. Source and receiver height were 0.4 m, the dictances are noted. Corresponding phase functions of the excess attenuation are shown below. Low frequencies are, relative to high frequencies, increasingly delayed with distance. The phase speed of the ground wave is smaller than the sound speed of a free wave.

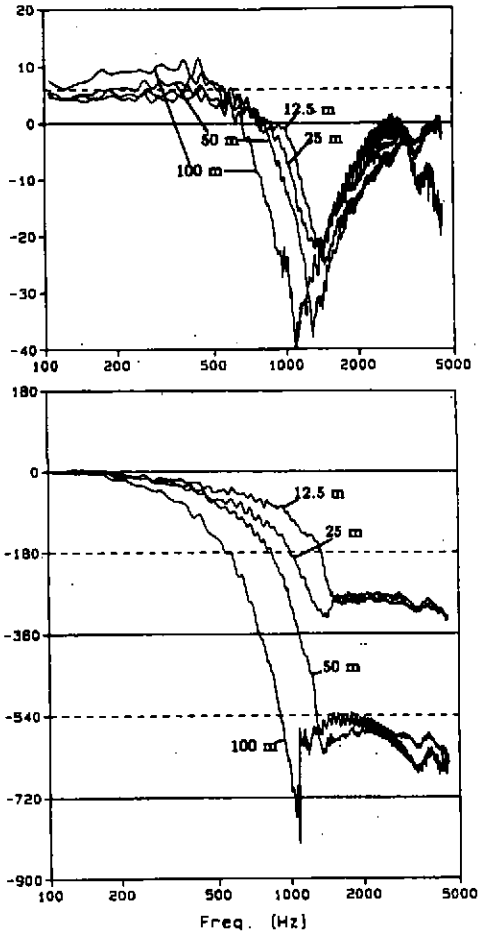

Fig. 2:
Magnitude of excess attenuation function for the same geometry as in Fig. 1, but during evening hours. The different meteorologic circumstances cause very different excess attenuation.
The corresponding phase functions are much stronger delayed than during the day, the phase speed of the ground wave has got smaller (Note the different scale).

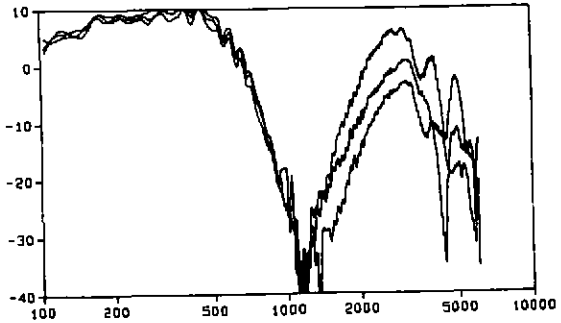

Fig.3:
Magnitude of the excess attenuation for three different wind conditions. The wind affects the reincrease of the functions towards high frequencies, which is due to path length difference. The ground wave part at low frequencies is not affected. The distance is 100 m, source and receiver height 0.4 m.

direct signal and reference signal). This linear part is estimated from the behaviour of the high frequency region, which is most sensitive to an overall time lag. It shows a nearly constant behaviour for all distances, high frequencies behave like spherical waves. The phase functions of low frequencies decrease up to the ground dip, increasingly fast with increasing distance. This behaviour is explained with the nature of the ground wave, which is coupled to the ground surface and travels with a phase speed smaller than free waves.

Influence of temperature gradients

Fig. 2 shows the strong influence of the different gradients during the two measurements at noon and towards evening. The measured functions exactly correspond in geometry to those in Fig. 1. They show a strong increase of the sound pressure level of high frequencies transmitted to each receiver position. The path length differences between direct and reflected sound do not decrease with increasing distance (they even increase for 50m and 100m), yielding a strong and nearly constant reincrease of the excess attenuation functions towards high frequencies. The sound pressure level of low frequencies exceeds +6 dB relative free propagation of a spherical wave for distances of 50 m and more. The phase delay of the ground wave is much larger than by day.
The differences in excess attenuation between day- and nighttime increase dramaticly with increasing distance. During day conditions, the ground gets more and more a high order low-pass filter with increasing distance, in the evening, it only attenuates through the marked ground dip while frequencies below and beyond are much better transmitted from source to receiver than expected from geometry.

Influence of varying wind

Even in a calm atmosphere, there are always slightly varying wind- and temperature fields, which scatter high frequent sound, yielding well audible changes in the sounding of a ground-near source. The main influence of the wind fluctuations establishes in the high frequency domain while low frequencies are not affected (→ Fig.3). The variations are due to changes in the path length difference between direct and reflected sound, which is responsible for the reincrease of the excess attenuation towards high frequencies. Depending on the wind situation, a more or less marked interference pattern is found at frequencies beyond the ground dip. The curves represent three measurements over 100 m, taken consecutively for a constant geometry. The time between the measurements is of the order 10 seconds, a single measurement is an average over a few (about 4) seconds, smoothened afterwards by averaging.

Explanation of the geometrical variations

A qualitative explanation of the measured effects can be given with the aid of the image of ray tracing. A positive sound speed gradient, i.e. temperature or wind speed increasing with height (downwind, evening temerature inversion) yields sound rays, which are bended towards the ground. The difference between the bended paths of direct and reflected waves increases with the sound speed gradient [2].

Small variations in the sound speed distribution, as they are caused by wind, lead to large variations in the sound speed gradient, hence to large variations in the path length difference, especially close to the ground, where the gradients usually are largest.

Negative gradients (during the day) yield a decrease of the path length difference, the rays are bended upward and a shadow region occurs [4]. The shadow region is penetrated by waves of low frequency, as long as their wavelength is large compared to the spatial dimensions of the gradients. The increase of the sound pressure level to more than +6 dB is explained by a focussing effect of the gradients. These two last statements can not be described in a quantitatively correct manor with a ray tracing method, because it does not account for the wave nature of sound.

THEORETICAL DESCRIPTION OF THE MEASUREMENTS

Provided the effective surface admittance and the geometry of the source–receiver configuration is known, the measured functions of excess attenuation can be calculated according to the well known theory of spherical wave reflection [1]. The measured functions are normalized to spherical spreading, they can be written as

$$H = 1 + \frac{r_1}{r_2} Q e^{ik\Delta r}, \tag{1}$$

where r_1 and r_2 are the path lengths of direct and refelcted waves, Δr is their difference, k is the wavenumber in air and Q is the reflection coefficient for spherical waves or the image source strength, respectively. A generally valid expansion for Q is [5]

$$Q = 1 + \frac{2\nu}{\sin\theta + \nu} i\sqrt{\pi}\rho_e e^{-\rho_e^2}\left[1 + \frac{2i\rho_e}{\sqrt{\pi}}\left(1 + \frac{\rho_e^2}{3} + \frac{\rho_e^4}{215} + \frac{\rho_e^6}{317} + \cdots\right)\right]; \quad \rho_e = \sqrt{\frac{ikr}{2}}(\sin\theta + \nu). \tag{2}$$

It is easily seen, that this series converges badly for large ρ_e, so for large numerical distances ρ_e, Q is easier calculated by

$$Q = 1 - \frac{2\nu}{\sin\theta + \nu}\left(1 - [1 - \operatorname{sign}(\Im m(\rho_e))]\, i\sqrt{\pi}\rho_e e^{-\rho_e^2} + \frac{1}{2\rho_e^2} + \frac{1\cdot 3}{(2\rho_e^2)^2} + \frac{1\cdot 3\cdot 5}{(2\rho_e^2)^3} + \cdots\right). \tag{3}$$

This latter expansion allows for a nice interpretation of the wave field to split up as a sum of sources of different order (monopole, dipole etc.) including a surface wave term, if ρ_e has a negative imaginary part, i.e. if $-\Im m(\nu) > \Re e(\nu) + \sin\theta$. For grazing incidence and strongly reactive admittancies, this surface wave dominates the ground wave, and an increases of the excess attenuation to more than +6dB is expected theoretically [5],[6]. This leads to the attempt of comparing the phase functions of the evening measurement with the wavenumber of the surface wave, $kr\nu^2/2$ [7]. The phases of the ground wave part decrease constantly for all distances, if they are depicted proportional to the parameter kr times frequency f (→ Fig. 4). Hence the admittance can be estimated to rise in magnitude proportional to the square root of frequency. This frequency dependence is the one

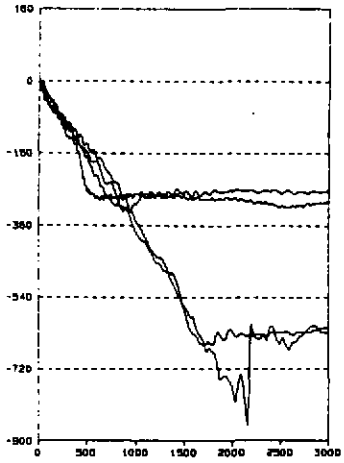

Fig. 4:
The phase functions of the evening measurement decrease about proportional to the frequency squared. They show a very similar behaviour, if they are depicted versus a parameter, which is proportional to kr times frequency. The four functions are reshown here versus kr $f/1000$. A comparision with the wavenumber of the surface wave, which is $kr\nu^2/2$, yields a value of the magnitude of the admittance, which is about 0.115 at 1 kHz and rises with the square root of frequency. The value of ν is confirmed by fits of the measured functions with the theory of spherical wave propagation, but the frequency dependence has to be stronger.

predicted for the ground to behave like an infinitely extended fibrous absorbent material. However, things are obviously more complicated. An attempt to fit the measured functions with such a frequency depending admittance fails in predicting the measured phase, as is shown in Fig. 5. A correct description of the frequency depending phase of the measured functions can only be achieved with an admittance which rises proportional to frequency. The assumption of the surface wave beeing the dominant part of the wave field is obviously incorrect for these measurements.

For the ground wave part of the measurements in discussion (frequency: 100 Hz → 1kHz), $\sqrt{\frac{kr}{2}}$ is in the range 3.5 → 35, $\sin\theta$ ranges from 0.15 to 0.01, and $|\nu|$ is of the order 0.01 → 0.1. A numerical comparision of the two series for Q shows a transition between them for $|\rho_s| \approx 3$. Consequently, the expansion in eq. (2) seems to be valid rather than thet in eq. (3). The behaviour of this series is extremely difficult to approximate, so the complete numerical solution has to be taken for the calculation of theoretical functions for Q.

The image source strength

In order to compare the measurements with calculated functions, it is convenient to eliminate the geometrical parameters in eq. (1). The ratio of path lengths r_1 and r_2 is practically equal to one for all geometries in question. Their difference Δr has a marked effect on the excess attenuation functions, because the ground dip is an interference minimum of the ground wave and the spherically diverging waves. Consequently, it is sensitively depending on the relative magnitude and phase lag of both. The effective path length difference for each measurement can be estimated from the reincrease of the magnitude towards high frequencies. The corresponding phase lag of the excess attenuation functions can be compensated for and the image source strenth itself can be calculated.

Discussion of measured image source strengths

The dependence of the theoretical image source strenth Q on the geometrical parameters is not easily seen in eq. (2) and eq. (3), so the measured behaviour for different grazing angles and different distances (these are the two geometrical input parameters of the equations) is compared to calculated predictions for a constant admittance. The admittance was set to an expression, which was found to give a satisfactory decription of the measurements: $\nu = 0.11\, f\, e^{-i \arctan(f^{0.75}/0.5)}$, f[kHz]. The linear dependence of the admittance on frequency is necessary for a correct fit of the phase functions, as

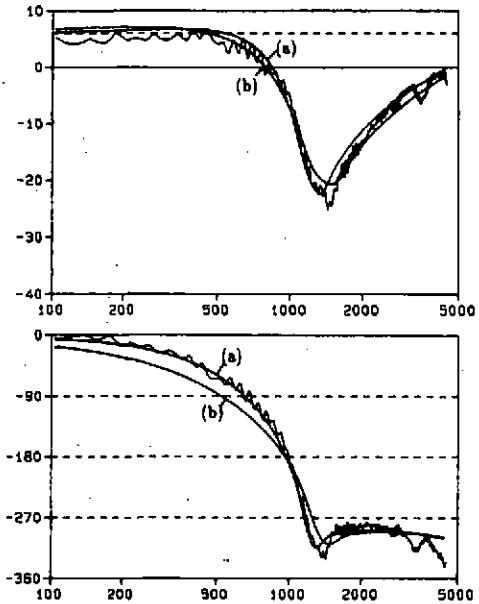

Fig. 5:
The evening measurement for 25m and $h_r = 0.4$ m is compared with two calculated functions, differing only in the frequency dependence of the magnitude of the admittance:

$$\nu = 0.1177 f^{n} e^{-i81°}; \quad f\,[kHz]$$

(a) : $\nu \sim f$, $x=1$
(b) : $\nu \sim \sqrt{f}$, $x=0.5$.

The magnitude of the excess attenuation is not very sensitive on the frequency dependence of the admittance, a fairly good fit is achieved with both models.
The phase function is much more sensitive, a linear increase gives a clearly better fit of the measured function.

shown above. The decrease of the phase angle of the admittance towards lower frequencies yields a better description of the small, but remarkable increase of the $|H|$–function in the low frequency domain. The measurements show an increasingly resistive behaviour of the ground for increasingly large wavelengths.

Angle dependence

Fig. 6 shows magnitude and phase lag of the image source strength calculated from evening measurements in 25 m distance and three receiver heights. The image has a value of around +1 for low frequencies and of −1 for high frequencies. This reflecting behaviour is to be expected for any surface at near grazing incidence, even for plane waves, but the increase of the measured magnitudes of the image source to values markedly larger than one can only be described with the reflection coefficient for spherical waves, or with the appearance of the ground wave, respectively. The maximum value of $|Q|$ increases with decreasing receiver height, i.e. with decreasing grazing angle. The peak is not shifted on the frequency axis, the phase functions decrease similarly.
The straight curves in Fig. 6 are calculated functions for the given geometry. The increase of the maximum with decreasing receiver height, which is a decrease of $\sin\theta$ as input parameter for the calculation of Q, is correctly described by theory.
In terms of the numerical distance, $\rho_s = \sqrt{ikr/2}(\sin\theta + \Re e\{\nu\} + i\Im m\{\nu\})$, the $\sin\theta$–term acts like an additional real part of the admittance, a decrease of $\sin\theta$ increases the phase angle of ρ_s, this increases the reactive behaviour of the ground, $|Q|$ gets larger [5].

Dependence on distance

Fig.7 shows the behaviour of Q for increasing distance and constant receiver height. The maximum value of $|Q|$ again increases with decreasing grazing angle. The maximum is shifted to lower frequencies with increasing kr. This shift is sensitive to the frequency dependence of the admittance. The straight curves in Fig.7 again represent calculated functions for the corresponding geometries.

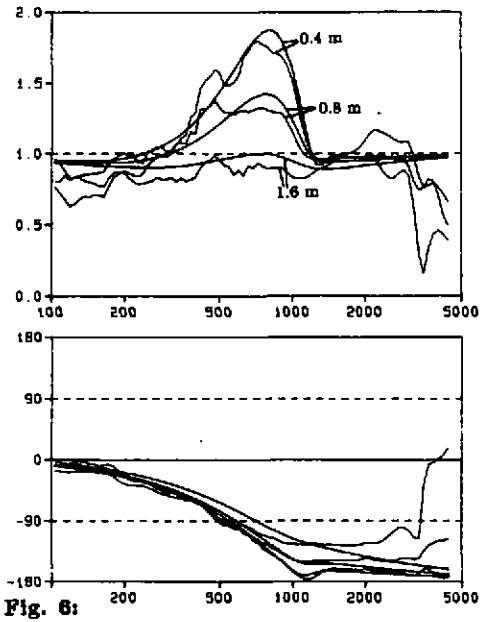

Fig. 6:
The magnitude and phase of the image source strength for three different receiver heights (noted) in a distance of 25 m. The magnitude has a strong maximum around 700 Hz, increasing with decreasing receiver height. The behaviour is correctly described by theory.

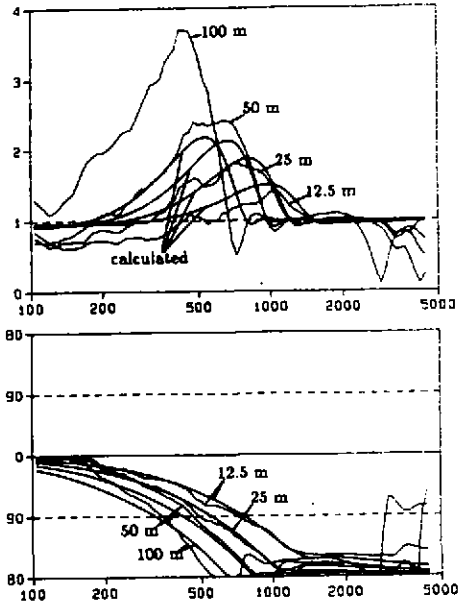

Fig. 7:
The maximum of the image strength is shifted to lower frequencies with increasing distance. The straight curves again represent theoretical functions, they underpredict the measured strong increase of $|Q|$ for 50 m and 100 m.

Apart from the measurement over 100 m, the measured shift of the negative slope of $|Q|$ is closely reproduced with a frequency proportional admittance.

A frequency dependence with a smaller exponent than one predicts a stronger dependence on distance. This can again be clarified by a look at the numerical distance. The location of the maximum on the frequency axis is mainly determined by the magnitude of ρ_s [6]. The magnitude is determined by the distance and $|\nu + \sin\theta|$, a variation of each of these factors acts in the same way on calculated functions. Provided a small grazing angle, the magnitude of the numerical distance can be written as $|\rho_s| = \sqrt{kr/2}|\nu(f)|^2$. The stronger the frequency dependence of the admittance, the smaller is the influence of the distance r, and vice versa, the strongest variation with distance is achieved with an admittance not depending on frequency.

The maximum of $|Q|$ is underestimated for 50 m and 100 m. A better fit of its height is achieved by a reduction of the effective grazing angle. A variation of this geometrical parameter should be allowed, particularly if the strong variations in the effective path length differences are remembered, which are caused by meteorological influences. However, the total shape of the calculated functions, especially the increase of $|Q|$ for low frequencies, gets even further away from the measured behaviour if the angle is altered.

Remarks on the noon measurement

All the statements given above hold for the evening measurement. Fits of the measurements, which were taken at noon, differ from the ones taken in the evening in the following way:

1. They show a less reactive behaviour of the ground, indicated by the behaviour of the excess attenuation, which does not exceed +6dB. A satisfactory fit of the measurements desires a smaller total phase of the numerical distance, which can be achieved either by a variation of the phase of the admittance or by an increase of the effective grazing angle.
2. Corresponding functions of $|Q|$ are shifted to higher frequencies. The location of the $|Q|$–maximum on the frequency axis is determined by the magnitude of the numerical distance. Hence its magnitude seems to be enlarged by meteorological effects, and this indicates a larger value of the effective surface admittance.
3. The phase functions for all distances again normalize with respect to the parameter $kr\ f$, like it is shown for the evening measurement in Fig. 4, but the dependence is much weaker. The phases decrease about proportional to $\sqrt{kr\ f}$. This empirical finding does not allow for a comparision of the phase functions with the wavenumber of the surface wave,but the theoretical phase of Q shows a nearly linear dependence on $|\rho_e|$. A comparision of $|\rho_e|$ with the measured phase function yields the reasonable value of 0.15 for the magnitude of the admittance at 1 kHs, again rising with the square root of frequency.

Conclusion

Measurements of the excess attenuation of sound, propagating close to a lawn surface, show large variations due to the meteorological circumstances even at small distances. The variations can partly be explained by a variation of geometrical parameters within the frame of the theory of spherical wave propagation. However, the described discrepancy in the frequency dependence of the measured phases indicates, that a correct model for the effective surface admittance of the outdoor ground has to accout for meteorological influences.

On the other hand, the finding of the measured phase functions to normalize with respect to $kr\ f$ gives rise to an attempt of finding empirically an expression for the ground wave itself. The influence of the ground and of meteorological parameters could be included in the effective properties of the ground wave, which could be handled as a more illustrated phenomenon, compared to dealing with the complicated theoretical expressions for the image source strength.

[1] *K. Attenborough, S.I.Hayek, J.M.Lawther. Propagation of sound above a porous half space.* **J.Acoust.Soc.Am. 68(5), 1493–1501, 1980.**

[2] *W.H.T. Huisman, M.J.M. Martens, W. van Asseldonk. Measured and Modelled Temperature Effects on Outdoor Sound Transmission.* **Institute of Acoustics 9, 1987.**

[3] *W. Wilken, J. Wempen. An FFT–based, High Resolution Measuring Technique with Application to Outdoor Ground Impedance at Grazing Incidence* **J.Noise Contr.Eng. 27(2), 52–60, 1986.**

[4] *M. E. Delany. Sound Propagation in the Atmosphere: A Historical Review.* **Acoustica 38, 201–223, 1977.**

[5] *J. Wempen. Sound Propagation Close to the Ground.*
Proceedings of the Workshop on Sound Propagation in Forested Areas and Shelterbelts, ed.: M.J.M.Martens, Katholic University, Nijmegen, The Netherlands, 83–92, 1986.

[6] *J. Wempen. Ground Effect on Long Range Sound Propagation* **Institute of Acoustics 9, 1987.**

[7] *K. Attenborough. Predicted Ground Effect for Highway Noise.* **J.Sound Vib. 81(3), 413–424, 1982.**